Electronic Supplementary Information

High Nuclearity Structurally - Related Mn Supertetrahedral T4 Aggregates

Katerina Skordi,[a] Antonis Anastassiades,[a] Adeline D. Fournet,[b] Rahul Kumar,[b] Michael Schulze,[c] Wolfgang Wernsdorfer,[c] George Christou,[b] Vassilios Nastopoulos,[d] Spyros P. Perlepes,[d] Constantina Papatriantafyllopoulou,*[e] and Anastasios J. Tasiopoulos*[a]

Department of Chemistry, University of Cyprus, 1678 Nicosia, Cyprus. Tel: ++357 22892765; E-mail: atasio@ucy.ac.cy

[b] *Department of Chemistry, University of Florida, Gainesville, Florida 32611-7200, United States.*

[c] *Institute of Quantum Materials and Technologies (IQMT), Hermann-von-Helmholtz-Platz 1, 76344, Eggenstein-Leopoldshafen, Germany.*

[d] *Department of Chemistry, University of Patras, Patras 26504, Greece.*

[e] *Synthesis and Solid-State Pharmaceutical Centre (SSPC), School of Chemistry, College of Science and Engineering, National University of Ireland Galway, University Road, H91 TK33, Galway, Ireland.*

Table of contents

Experimental Section..... 2 – 6

Discussion for the synthesis and crystal structures of **1** – **3**.....7 – 8

Bond valence sum calculations for the Mn and O atoms of **1** – **3**..... 9 – 14

Structural figures of **1** – **3**..... 15 – 22

Magnetism plots of **1** – **3**..... 23 – 28

References..... 29

Experimental section

Materials

All manipulations were performed under aerobic conditions using reagents and solvents as received. $Mn(EtCO_2)\cdot 2H_2O$[1] and NBu_4MnO_4[2] were prepared as previously described.

Syntheses

$[Mn_{24}O_{14}(OH)_2\{(py)_2CO_2\}_8(pd)_6(MeCO_2)_4(NO_3)_{0.5}(H_2O)_{4.1}](NO_3)_{1.3}(OH)_{2.2}$ (1) Solid $Mn(NO_3)_2\cdot 4H_2O$ (0.75 g, 2.99 mmol) was added to a stirred solution of H_2pd (0.30 mL, 0.32 g, 4.15 mmol) and NEt_3 (0.28 mL, 0.20 g, 2.01 mmol) in EtOH (20 mL) and the resulting brown solution was left under magnetic stirring for 5 min. To this solution was added solid $(py)_2CO$ (0.10 g, 0.54 mmol), and $MeCO_2Na$ (0.08 g, 0.98 mmol) under continuous stirring. The resulting brown solution was stirred for 1 hour, filtered off and the filtrate was left undisturbed in an open flask, at room temperature. Slow evaporation of the solvent at room temperature gave dark brown crystals after ~ eight weeks of **1**$\cdot 2.5H_2O\cdot$solvent, which were kept in mother liquor for X-ray analysis, or collected by filtration and dried under vacuum for other solid-state studies. Yield: ~55%. Vacuum-dried solid analyzed (C, H, N) as **1**$\cdot 22H_2O$. Calcd. (Found): C, 30.58 (30.98); H, 3.79 (3.76); N, 5.57 (5.32) %. Selected IR data (KBr, cm^{-1}): 3412(mb), 3134(mb), 3020(m), 2853(w), 2779(w), 1616(m), 1400(s), 1242(w), 1155(w), 1117(w), 1074(w), 1053(w), 816(w), 775(w), 694(w), 667(m), 621(m), 561(w), 534(w), 476(w).

$[Mn_{23}O_{13}(OH)\{(py)_2C(O)_2\}_6(pd)_7(MeCO_2)_6(H_2O)_6](OH)_5$ (2). It was prepared from the same procedure followed for **1** with the use of MeCN (20 mL) as reaction solvent instead of EtOH. Yield: ~60%. Vacuum-dried solid analyzed (C, H, N) as **2**$\cdot 33H_2O$. Calcd. (Found): C, 27.33 (27.02); H, 4.45 (4.80); N, 3.86 (4.01) %. Selected IR data (KBr, cm^{-1}): 3391(mb), 3154(mb), 2920(w), 2851(w), 2779(w), 1597(w), 1475(m), 1398(s), 1385(s), 1252(w), 1155(w), 1115(w), 1073(w), 1047(m), 1016(m), 975(w), 814(w), 785(w), 764(w), 694(m), 648(m), 630(m), 604(m), 577(m), 554(m), 515(w), 474(w), 409(w).

$[Mn_{23}O_{13}(OH)\{(py)_2C(O)_2\}_6\{(py)_2C(OH)_2\}_{0.25}(pd)_7(EtCO_2)_6(H_2O)_{5.25}](OH)_{4.25}(NO_3)_{0.75}$ (3). It was prepared from the same procedure followed for **2** with the differences that the reaction took

place in a different solvent (2-PrOH instead of MeCN) and $EtCO_2Na$ was used in place of $MeCO_2Na$. Yield: ~60%. Vacuum-dried solid analyzed (C, H, N) as **3**·$28H_2O$. Calcd. (Found): C, 29.31 (29.02), H, 4.43 (4.35), N, 4.20 (4.31) %. Selected IR data (KBr, cm^{-1}): 3412(mb), 3134(mb), 3020(m), 2853(w), 2779(w), 1606(m), 1405(s), 1385(s), 1242(w), 1155(w), 1117(w), 1074(w), 1053(w), 980(w), 816(w), 775(w), 694(w), 667(m), 621(m), 561(w), 534(w), 476(w), 401(w).

X-ray Crystallography

Data were collected on a Rigaku-Oxford Diffraction SuperNova diffractometer equipped with a CCD area detector and a graphite monochromator utilizing Cu Kα (λ= 1.5418 Å) (for compounds **1** and **2**) or Mo Kα (λ= 0.71073 Å) (for compound **3**) radiation. Selected crystals were attached to glass fiber with paratone-N oil and transferred to a goniostat for data collection. Empirical absorption corrections (multiscan based on symmetry - related measurements) were applied using CrysAlis RED software.[3] The same software package was used for data collection, cell refinement and data reduction. The structures were solved by direct methods using either SIR2014[4] or SHELXS,[5] via the WinGX[6] interface. They were refined on F^2 using full-matrix least-squares with SHELXL-2018/3[7] and OLEX2[8] package. DIAMOND[9] and MERCURY[10] were used for molecular graphics. For all compounds multiple datasets were collected with single crystals produced from various different crystallization experiments and structure determination was eventually carried out by means of the best data set collected. For compound **2** crystal data are of moderate/low quality and as a result, some atoms exhibit higher than usual thermal ellipsoids. However, the connectivity of the complexes was clearly determined and the structure was normally refined. The non-H atoms were treated anisotropically, whereas the carbon-bound H-atoms were placed in calculated ideal positions and refined as riding on their respective parent atoms. In all three compounds, the H-atoms of coordinated and lattice H_2O molecules with full occupancies were located in difference Fourier maps and refined isotropically applying soft distance restraints (DFIX/DANG). The H-atoms of solvent H_2O molecules with partial occupancies and those involved in substitutional disorder in compounds **1** and **3**, together with those of a disordered $(py)_2C(OH)_2$ ligand with 0.25 occupancy in **3**, could not be properly located (or refined with a chemically reasonable geometry). It was proven difficult to develop an atomistic model of the remaining highly disordered solvent molecules

(mostly H_2O) and, therefore, their electron density contribution was removed (in all three compounds) from the intensity data using the SQUEEZE function from the PLATON software suit.[11] The number of these latter solvents, based on the count of the removed electrons, the volume of the corresponding masked regions and visual inspection of the difference density maps, is estimated to be ~ 20 H_2O for the structure of **1** and ~ 25 H_2O per complex for the structures of **2** and **3**.

A highly disordered nitrate ion, with an estimated occupancy of 0.60, was also removed from compound **1**. Non-routine aspects of structure refinement are as follows: i) complex **1** exhibits substitutional disorder of the N17/O32/O58/O59 nitrate ion and O32 water molecule coordinated to Mn1 with site-occupancy factors of 0.50:0.50; one pd^{2-} ligand is also positionally disordered and was modeled in two orientations: O28-C106-C105-C104-O27 and O28-C106-C205-C204-O43 with a 75:25 domain ratio, respectively, ii) one pd^{2-} ligand in complex **2** is orientationally disordered about a three-fold axis passing through Mn1 atom of the complex, iii) substitutional disorder was observed in complex **3** between a $(py)_2C(OH)_2$ ligand coordinated to Mn1 and a nearby nitrate ion and were refined with site-occupancy factors of 0.25 and 0.75, respectively; three pd^{2-} and three propionate ligands were also positionally disordered and have been modelled over two positions. Geometrical and ADP restraints have been applied in order to handle the mentioned disorder of the organic ligands in **1**−**3**. Selected lattice O atoms (2.2 in compound **1**, 5 in compound **2** and 4.25 in **3**) were assigned as OH^- anions to balance the positive charges in the reported compounds. Appropriate responses for various checkcif alerts are incorporated in the cif files, most of them due to the low quality of the data (**2**), the complexity of the molecules (displaying high nuclearities, significant molecular weights and large unit cell volumes up to 92314 $Å^3$ as in **3**), and disorder of the ligands. Selected crystal data for all three compounds are summarized in Table S1.

Physical Studies.

Elemental analysis (C, H, N) was performed by the in-house facilities of the University of Cyprus, Chemistry Department. Infrared spectra were recorded in the solid state (KBr pellets) on a Shimadzu Prestige-21 spectrometer in the 4000−400 cm^{-1} range. Variable-temperature dc and ac magnetic susceptibility data were collected at the University of Florida using a Quantum Design MPMS-XL SQUID susceptometer equipped with a 7 T magnet and operating in the

1.8−300 K range. Samples were embedded in solid eicosane to prevent torquing. The ac magnetic susceptibility measurements were performed in an oscillating ac field of 3.5 G and a zero dc field. The oscillation frequencies were in the 5−1488 Hz range. Pascal's constants were used to estimate the diamagnetic corrections, which were subtracted from the experimental susceptibilities to give the molar paramagnetic susceptibility (χ_M).

Table S1. Selected crystal data for compounds **1**·2.5H_2O·solvent - **3**·3.8H_2O·solvent.

Parameter	**1**·2.5H_2O	**2**·3H_2O	**3**·3.8H_2O
Empirical formula	$C_{114}H_{129.4}Mn_{24}N_{17.2}O_{64.40}$	$C_{99}H_{127}Mn_{23}N_{12}O_{61}$	$C_{107.75}H_{145.85}Mn_{23}N_{13.25}O_{68.05}$
Formula weight	4089.50	3724.74	3979.19
Crystal system	triclinic	cubic	trigonal
Space group	P $\bar{1}$	P a □	R □
Unit cell dimensions			
a (Å)	18.4677(8)	31.9384(9)	42.7113(9)
b (Å)	19.8514(8)	31.9384(9)	42.7113(9)
c (Å)	25.7641(7)	31.9384(9)	58.4319(8)
α(°)	67.980(3)		
β(°)	85.789(3)		
γ(°)	87.810(4)		
V (Å^3)	8732.1(6)	32579(3)	92314(4)
Z	2	8	18
ρ_{calc} (g cm^{-3})	1.555	1.518	1.283
λ (Å)	1.54184	1.54184	0.71073
μ (mm^{-1})	14.276	14.620	1.428
T (K)	100(2)	100(2)	100(2)
Measured/independent reflections (R_{int})	61170/31082 (0.0637)	26165/9675 (0.1452)	56077/36048 (0.0293)
Parameters refined	2076	614	2073
Gof (on F^2)	0.952	0.879	1.037
R_1[a] ($I > 2\sigma(I)$)	0.0666	0.1131	0.0720
wR_2[b] ($I > 2\sigma(I)$)	0.1724	0.2670	0.2171
$(\Delta\rho)_{maximum}/(\Delta\rho)_{minimum}$ (e Å^{-3})	1.935/-0.579	0.779/-0.643	2.682/-0.662

[a] $R_1=\Sigma \| Fo \| - | Fc \| / \Sigma | Fo |$. [b] $wR_2(F^2)=[\Sigma[w(F_o^2 - F_c^2)2]/\Sigma[wF_o^2)2]]^{1/2}$, $w=1/[\sigma^2(F_o^2) + (m\cdot p)^2 + n\cdot p]$, $p=[\max(F_o^2,0) + 2F_c^2]/3$, and m and n are constants.

Discussion for the synthesis of compounds 1 - 3. Our group has been investigating the use of 1,3-propanediol (pdH_2) in Mn cluster chemistry targeting to new polynuclear compounds with interesting crystal structures and magnetic properties. These studies have led to the isolation of several metal clusters including high nuclearity ones such as $[Mn_{44}]$, $[Mn_{40}Na_4]$, $[Mn_{36}Ni_4]$ aggregates and others.[12,13] An extension of these studies included the investigation of 1,3-pdH_2 in combination with other chelating ligands, such as di-2-pyridyl ketone ($(py)_2CO$), which provided access to new compounds including a family of homometallic $[Mn_6]$ and heterometallic $[Mn_4Ln_2]$ (Ln = Dy, Gd, Tb) species that contain both ligands.[14] This success prompted us to investigate further this reaction system by employing various synthetic approaches targeting to additional high nuclearity clusters from the combination of pdH_2 and ($(py)_2CO$). Thus, the reaction of $Mn(NO_3)_2{\cdot}4H_2O$, pdH_2 and $(py)_2CO$ in the presence of NEt_3 and $MeCO_2Na$ in a molar ratio of ~ 1 : 1.4 : 0.2 : 0.7 : 0.3 in EtOH eventually led to dark brown crystals of $[Mn_{24}O_{14}(OH)_2\{(py)_2CO_2\}_8(pd)_6(MeCO_2)_4(NO_3)_{0.5}(H_2O)_{4.1}](NO_3)_{1.3}(OH)_{2.2}$ (**1**) after several weeks. Various modifications were performed in this reaction to investigate in detail this reaction system including the use of different solvents, carboxylate sources, etc. Thus, when the above discussed reaction was repeated in MeCN instead of EtOH the product was compound $[Mn_{23}O_{13}(OH)\{(py)_2C(O)_2\}_6(pd)_7(MeCO_2)_6(H_2O)_6](OH)_5$ (**2**). A similar reaction but by employing $EtCO_2Na$ instead of $MeCO_2Na$ and 2-propanol instead of MeCN provided access to $[Mn_{23}O_{13}(OH)\{(py)_2C(O)_2\}_6\{(py)_2C(OH)_2\}_{0.25}(pd)_7(EtCO_2)_6(H_2O)_{5.25}](OH)_{4.25}(NO_3)_{0.75}$ (**3**). In all these reactions, the oxidation state of the starting material ($Mn(NO_3)_2{\cdot}4H_2O$) is 2+, whereas the average oxidation state of the final products is higher (since **1**-**3** are mixed valent Mn^{II}/Mn^{III} compounds) although no oxidant was added in the reaction mixture. We believe that the atmospheric O_2 is responsible for this oxidation which is facilitated by the existence of bases (Et_3N and $MeCO_2Na$ or $EtCO_2Na$) in the reaction mixtures as it has also been observed in the past.[15] Further reactions using different solvents, bases, and carboxylate ligands were also investigated but resulted in amorphous precipitates that could not be further characterised. The reaction system was proven to be sensitive even at minor alternations of the reaction conditions, which is often the case for Mn cluster chemistry.[16] It is clear that the overall reactions are very complicated, and the reaction solution probably contains a mixture of various compounds in equilibrium, with factors including relative solubility, lattice energies, crystallization kinetics,

and others determining the identity of the isolated product. One (or more) of these factors is likely the reason that by changing the solvent from MeOH to EtOH or to 2-propanol or the carboxylate used from acetate to propionate, a variety of different products were formed.

Discussion for the crystal structures of compounds 1 - 3. A detailed description of the crystal structures of **1**-**3** is included in the main manuscript. Below is summarized information about the extended structures of the three compounds and the hydrogen bonding interactions which due to lack of space could not be included in the main text. In particular, a close examination of the packing of **1**-**3** revealed that there are no direct hydrogen bonding interactions between the metal clusters. As a result, the clusters are fairly well isolated with the shortest Mn···Mn separation between metal ions of neighboring units appearing in the case of compound **3** being 7.895 Å. However, there are in all three clusters hydrogen bonding interactions involving ligated molecules, lattice water molecules and counter anions. This supramolecular connection through coordinated/solvent water molecules and counter anions is demonstrated for the case of compound **1** in Figure S3.

Table S2. Bond Valence Sum calculations for the Mn atoms in complex **1.**[a]

	Mn(II)	Mn(III)	Mn(IV)
Mn1	3.11	**2.88**	2.97
Mn2	**1.89**	1.76	1.80
Mn3	3.26	**2.98**	3.13
Mn4	3.22	**2.94**	3.09
Mn5	**1.90**	1.77	1.81
Mn6	3.23	**2.95**	3.10
Mn7	3.65	**3.34**	3.50
Mn8	3.11	**2.84**	2.99
Mn9	3.22	**2.95**	3.10
Mn10	3.18	**2.91**	3.06
Mn11	3.19	**2.92**	3.07
Mn12	3.12	**2.86**	3.00
Mn13	**2.01**	1.87	1.91
Mn14	3.05	**2.79**	2.93
Mn15	3.12	**2.86**	3.00
Mn16	**2.03**	1.86	1.95
Mn17	**2.09**	1.92	2.01
Mn18	3.24	**3.01**	3.09
Mn19	3.29	**3.04**	3.14
Mn20	3.20	**2.97**	3.04
Mn21	3.18	**2.91**	3.06
Mn22	3.09	**2.83**	2.97

Mn23	3.35	**<u>3.06</u>**	3.21
Mn24	**<u>1.97</u>**	1.83	1.87

[a] The underlined value is the one closest to the charge for which it was calculated.

Table S3. Bond Valence Sum calculations for the O atoms in complex **1.**

	BVS	Protonation Level		BVS	Protonation Level		BVS	Protonation Level
$(py)_2C(O)_2^{2-}$			**pd^{2-}**			**μ_4-O^{2-}**		
O1	1.49	**RO^-**	**O17**	1.85	**RO^-**	**O7**	1.73	**O^{2-}**
O2	1.91	**RO^-**	**O18**	1.80	**RO^-**	**O42**	1.97	**O^{2-}**
O3	1.59	**RO^-**	**O19**	1.79	**RO^-**	**O44**	1.93	**O^{2-}**
O4	1.83	**RO^-**	**O20**	1.82	**RO^-**	**O45**	1.72	**O^{2-}**
O5	1.82	**RO^-**	**O21**	1.85	**RO^-**	**O46**	1.89	**O^{2-}**
O6	1.62	**RO^-**	**O22**	1.85	**RO^-**	**O47**	1.92	**O^{2-}**
O8	1.54	**RO^-**	**O23**	1.92	**RO^-**	**O48**	1.93	**O^{2-}**
O56	1.95	**RO^-**	**O24**	1.94	**RO^-**	**O49**	2.00	**O^{2-}**
O9	1.85	**RO^-**	**O25**	1.84	**RO^-**	**O50**	1.83	**O^{2-}**
O10	1.72	**RO^-**	**O26**	1.82	**RO^-**	**O54**	1.85	**O^{2-}**
O11	1.62	**RO^-**	**O27**	1.86	**RO^-**	**μ_3-O^{2-}**		
O12	1.86	**RO^-**	**O28**	1.85	**RO^-**	**O41**	1.90	**O^{2-}**
O13	1.85	**RO^-**	**H_2O**			**O51**	1.86	**O^{2-}**
O14	1.68	**RO^-**	**O29**	0.27	**H_2O**	**O52**	1.77	**O^{2-}**
O15	1.92	**RO^-**	**O30**	0.32	**H_2O**	**O53**	1.79	**O^{2-}**
O16	1.65	**RO^-**	**O31**	0.37	**H_2O**	**μ_3-OH^-**		
			O32	0.30	**H_2O**	**O43**	0.85	**OH^-**
						O55	0.96	**OH^-**

Table S4. Bond Valence Sum calculations for the Mn atoms in complex **2.**[a]

	Mn(II)	Mn(III)	Mn(IV)
Mn1	3.43	**3.17**	3.27
Mn2	3.12	**2.85**	3.00
Mn3	3.12	**2.85**	3.00
Mn4	3.21	**2.94**	3.08
Mn5	3.18	**2.91**	3.05
Mn6[b]	**2.60**	**2.38**	2.49
Mn7	**1.96**	1.83	1.87
Mn8	3.30	**3.07**	3.14
Mn9	**1.64**	1.50	1.57

[a] The underlined value is the one closest to the charge for which it was calculated.

[b] The obtained bond valence sum values for Mn6 lie between the expected values for oxidation states 2+ and 3+ but deviate significantly from them. This indicates the possibility that Mn6 is a mixed valent (2+/3+) site (totally three symmetry – related ions). It is noted that Mn6 is coordinated to six oxygen atoms displaying a distorted octahedral coordination environment and the Mn-O bond lengths range from 1.970 (10) – 2.245(10) Å. The average Mn−O bond length of 2.083 Å is smaller than the typical Mn^{II}−O bond lengths[b1] and larger than the common Mn^{III}−O bond lengths[b2].

[b1] For example, the Mn – O bond lengths of the Mn^{II} ions in compound **2** are as follows: Mn7: 2.084 – 2.323 Å, average Mn – O bond length: 2.166 Å; Mn9: 2.228 – 2.372 Å, average Mn – O bond length: 2.310 Å. In addition, the Mn – O bond lengths of the Mn^{II} ions in compound **1** are as follows: Mn2 2.173 – 2.421 Å, average Mn – O bond length: 2.265 Å; Mn5 2.125 – 2.271 Å, average Mn – O bond length: 2.185 Å; Mn13 2.055 – 2.297 Å average Mn – O bond length: 2.166 Å; Mn16 2.131 – 2.275 Å average Mn – O bond length: 2.169 Å; Mn17 2.114 – 2.273 Å average Mn – O bond length: 2.158 Å; Mn24 2.071 – 2.310 Å average Mn – O bond length: 2.169 Å.

[b2] For example, the Mn – O bond lengths of the Mn^{III} ions in compound **2** are as follows: Mn1 1.977 – 1.998 Å average Mn – O bond length: 1.988 Å; Mn2 1.884 – 2.253 Å average Mn – O bond length: 2.033 Å; Mn3 1.857 – 2.426 Å average Mn – O bond length: 2.055 Å; Mn4 1.888 – 2.339 Å average Mn – O bond length: 2.029 Å; Mn5 1.865 – 2.376 Å average Mn – O bond length: 2.052 Å; Mn8 1.863 – 2.250 Å average Mn – O bond length: 2.035 Å. In addition, the

Mn – O bond lengths of the Mn^{II} ions in compound **1** are as follows: Mn1 1.887 – 2.155 Å, average Mn – O bond length: 1.971 Å; Mn3 1.856 – 2.427 Å, average Mn – O bond length: 2.048 Å; Mn4 1.857 – 2.320 Å, average Mn – O bond length: 2.039 Å; Mn6 1.852 – 2.291 Å, average Mn – O bond length: 2.033 Å; Mn7 1.907 – 2.048 Å, average Mn – O bond length: 1.952 Å; Mn8 1.867 – 2.496 Å, average Mn – O bond length: 2.047 Å; Mn9 1.899 – 2.267 Å, average Mn – O bond length: 2.019 Å; Mn10 1.868 – 2.277 Å, average Mn – O bond length: 2.033 Å; Mn11 1.847 – 2.332 Å, average Mn – O bond length: 2.046 Å; Mn12 1.891 – 2.336 Å, average Mn – O bond length: 2.049 Å; Mn14 1.874 – 2.387 Å, average Mn – O bond length: 2.059 Å; Mn15 1.892 – 2.283 Å, average Mn – O bond length: 2.041 Å; Mn18 1.862 – 2.132 Å, average Mn – O bond length: 1.962 Å; Mn19 1.866 – 2.071 Å, average Mn – O bond length: 1.933 Å; Mn20 1.884 – 2.205 Å, average Mn – O bond length: 1.997 Å; Mn21 1.912 – 2.283 Å, average Mn – O bond length: 2.023 Å; Mn22 1.876 – 2.460 Å, average Mn – O bond length: 2.067 Å; Mn23 1.911 – 2.062 Å, average Mn – O bond length: 1.985 Å.

Table S5. Bond Valence Sum calculations for the O atoms in complex **2**.

	BVS	**Protonation Level**		**BVS**	**Protonation Level**
$(py)_2C(O)_2^{2-}$			**μ_4-O^{2-}**		
O1	1.80	**RO^-**	**O16**	1.80	**O^{2-}**
O2	1.54	**RO^-**	**O17**	1.84	**O^{2-}**
O3	1.79	**RO^-**	**O18**	1.99	**O^{2-}**
O4	1.94	**RO^-**	**O19**	1.98	**O^{2-}**
pd^{2-}			**μ_3-O^{2-}**		
O5	1.91	**RO^-**	**O20**	1.81	**O^{2-}**
O6	1.75	**RO^-**	**μ_3-OH^-**		
O7	1.89	**RO^-**	**O13**	0.99	**OH^-**
O8	1.85	**RO^-**	**H_2O**		
O13	1.94	**RO^-**	**O14**	0.24	**H_2O**
			O15	0.19	**H_2O**

Table S6. Bond Valence Sum calculations for the Mn atoms in complex **3**.[a]

	Mn(II)	Mn(III)	Mn(IV)
Mn1	**1.94**	1.80	1.84
Mn2	3.18	**2.91**	3.06
Mn3	3.23	**2.95**	3.10
Mn4	3.26	**2.98**	3.13
Mn5[b]	2.63	**2.40**	2.52
Mn6	3.22	**2.94**	3.09
Mn7[b]	2.90	**2.65**	2.78
Mn8	3.22	**2.95**	3.10
Mn9[b]	**2.48**	2.27	2.38
Mn10	3.21	**2.94**	3.09
Mn11	3.13	**2.86**	3.00
Mn12	3.09	**2.83**	2.97
Mn13	3.13	**2.86**	3.00
Mn14	3.28	**3.04**	3.12
Mn15	3.07	**2.80**	2.94
Mn16	3.29	**3.01**	3.16
Mn17	3.15	**2.88**	3.02
Mn18	3.07	**2.80**	2.94
Mn19	**1.91**	1.77	1.81
Mn20	3.34	**3.10**	3.18
Mn21	**1.92**	1.79	1.83
Mn22	2.91	**2.69**	2.78
Mn23	**1.70**	1.59	1.62

[a] The underlined value is the one closest to the charge for which it was calculated.

[b] BVS calculations for the Mn atoms of compound **3** indicate the difficulty to determine the oxidation state of the Mn5, Mn7 and Mn9 centers (these Mn ions correspond to the Mn6 symmetry-related ions of **2**). Among them, it is clear that Mn7 can be assigned as a Mn^{3+} ion

whereas there is still uncertainty for the oxidation states of Mn5 (BVS values of 2.63 and 2.40 assuming oxidation state values 2+ and 3+, respectively) and Mn9 (BVS values of 2.48 and 2.27 assuming oxidation state values 2+ and 3+, respectively). We assign Mn5 as a Mn^{3+} ion and Mn9 as a Mn^{2+} ion since their BVS values are closer to these expected for oxidation states 3+ and 2+, respectively. This in turn provides an additional evidence that Mn6 atom af the analogous Mn_{23}-acetate compound is a mixed valent site suggesting a 0.66 Mn^{3+} / 0.33 Mn^{2+} situation.

Table S7. Bond Valence Sum calculations for the O atoms in complex **3**.

	BVS	Protonation Level		BVS	Protonation Level		BVS	Protonation Level
$(py)_2C(O)_2^{2-}$			**pd^{2-}**			**μ_4-O^{2-}**		
O1	1.87	**RO^-**	**O17**	1.95	**RO^-**	**O47**	1.82	**O^{2-}**
O2	1.65	**RO^-**	**O18**	1.97	**RO^-**	**O48**	2.01	**O^{2-}**
O3	1.87	**RO^-**	**O19**	1.81	**RO^-**	**O49**	1.81	**O^{2-}**
O4	1.71	**RO^-**	**O20**	1.98	**RO^-**	**O50**	1.76	**O^{2-}**
O5	1.87	**RO^-**	**O25**	1.90	**RO^-**	**O51**	1.81	**O^{2-}**
O6	1.62	**RO^-**	**O26**	2.03	**RO^-**	**O52**	1.96	**O^{2-}**
O7	1.91	**RO^-**	**O29**	1.85	**RO^-**	**O53**	1.72	**O^{2-}**
O8	1.68	**RO^-**	**O30**	1.78	**RO^-**	**O54**	1.95	**O^{2-}**
O9	1.64	**RO^-**	**O31**	1.85	**RO^-**	**O55**	1.74	**O^{2-}**
O10	1.86	**RO^-**	**O32**	1.79	**RO^-**	**O56**	1.94	**O^{2-}**
O11	1.68	**RO^-**	**O33**	1.79	**RO^-**	**μ_3-O^{2-}**		
O12	1.92	**RO^-**	**O34**	1.75	**RO^-**	**O57**	1.79	**O^{2-}**
$(py)_2C(OH)_2$			**O36**	1.81	**RO^-**	**O58**	1.77	**O^{2-}**
O40	1.11	**ROH**	**O37**	1.82	**RO^-**	**O59**	1.78	**O^{2-}**
O41	0.89	**ROH**	**H_2O**			**μ_3-OH^-**		
			O40	0.23	**H_2O**	**O35**	0.97	**OH^-**
			O42	0.24	**H_2O**			
			O43	0.23	**H_2O**			
			O60	0.33	**H_2O**			
			O61	0.31	**H_2O**			
			O62	0.32	**H_2O**			

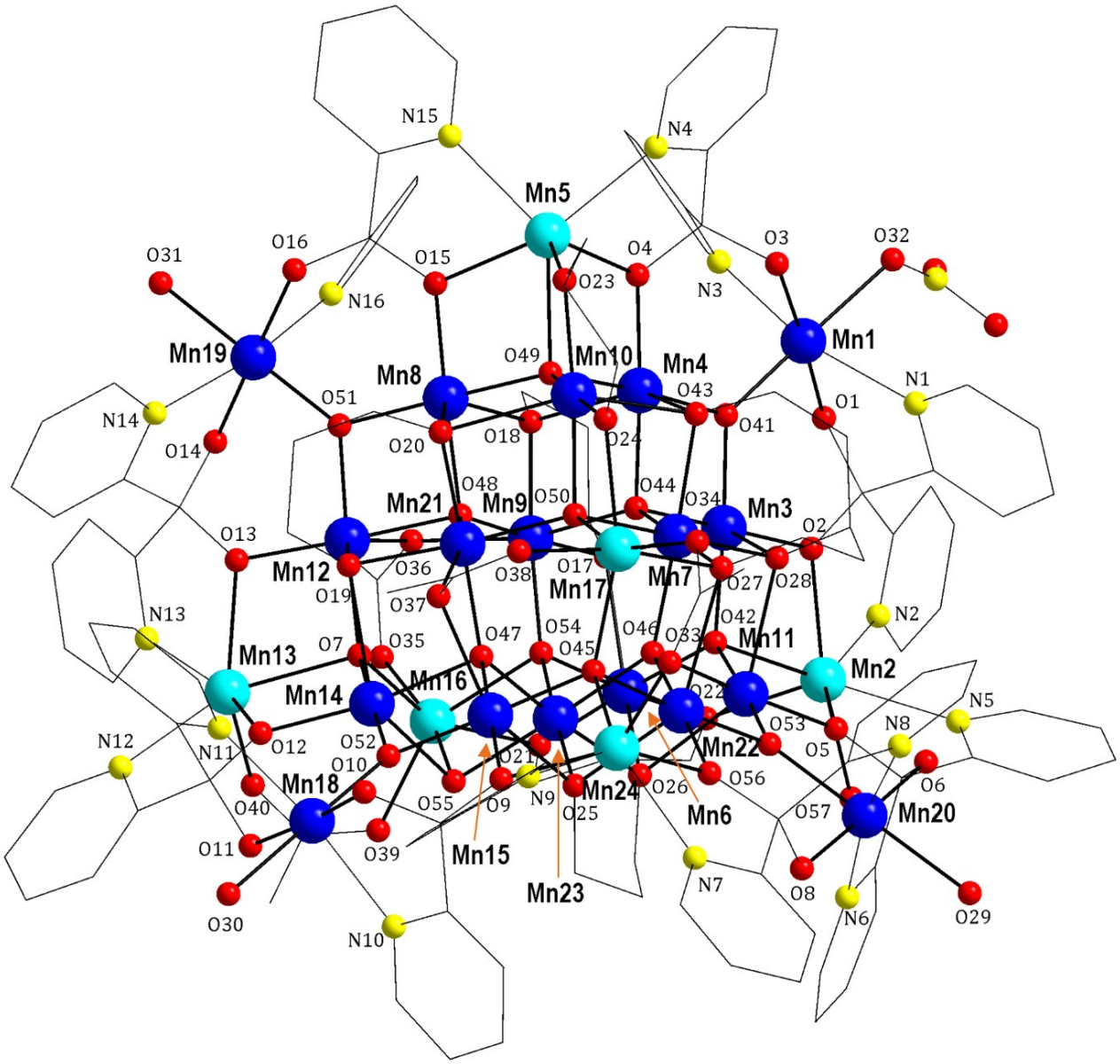

Fig. S1. Partially labeled representation of the molecular structure of the cation of **1**. Colour code: Mn^{II}, turqoise; Mn^{III}, blue; O, red; N, yellow; C, grey. H atoms and the counter ions are omitted for clarity.

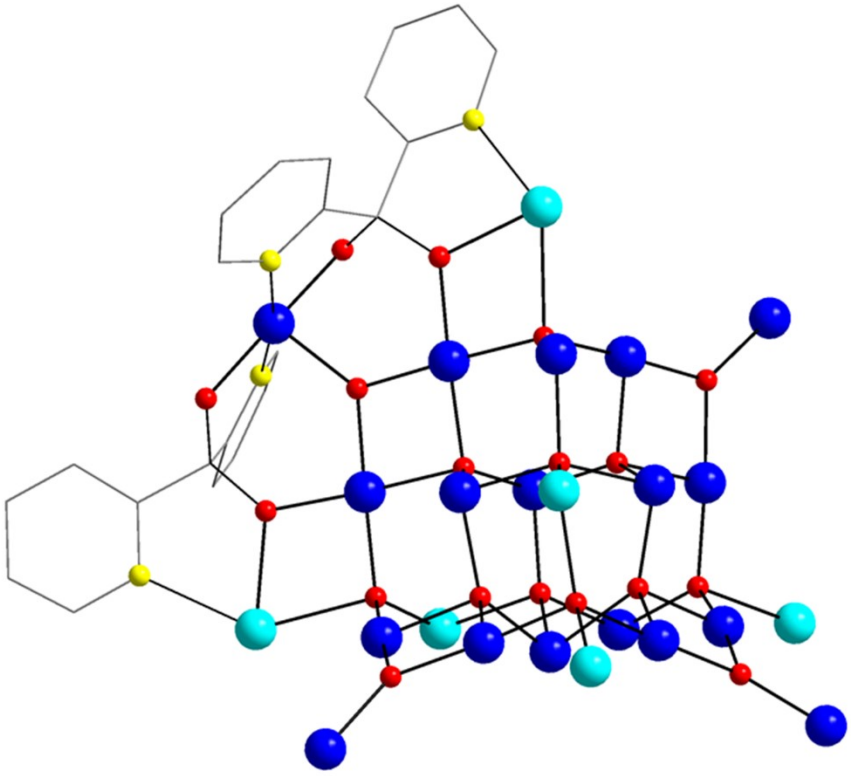

Fig. S2. The connection of the [Mn_{20}] supertetrahedral T4 core of the cation of **1** with a capping Mn^{III} ion through a pair of $\eta^1:\eta^2:\eta^1:\eta^1:\mu_3$ $(py)_2C(O)_2^{2-}$ ligands. Colour code: Mn^{II}, turqoise; Mn^{III}, blue; O, red; N, yellow; C, grey. H atoms are omitted for clarity.

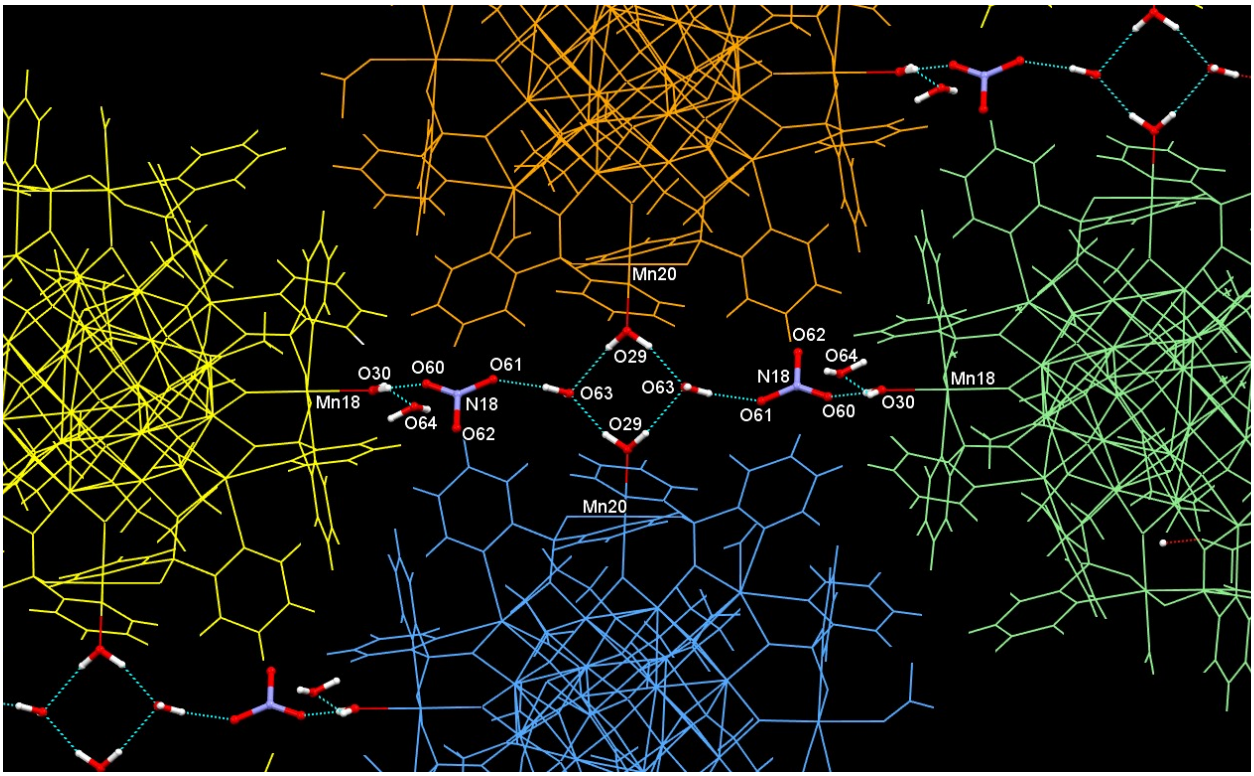

Fig S3. Representation of parts of adjacent [Mn_{24}] cations and lattice solvent molecules and counter anions of **1** emphasizing on the supramolecular assembly of the clusters mediated by H-bonds between the coordinated/solvent water molecules and the nitrate counter anions.

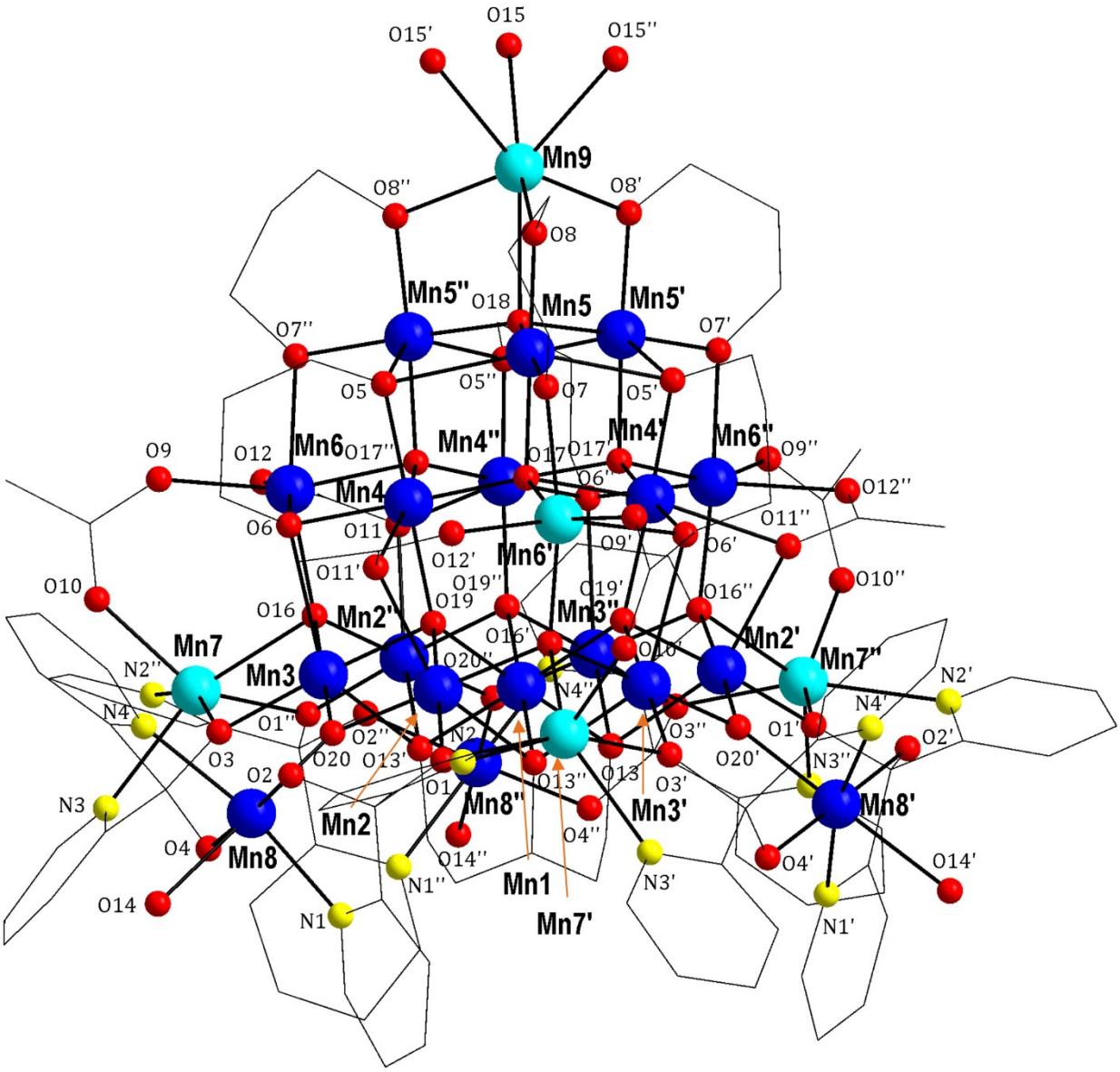

Fig. S4. Partially labeled representation[a] of the molecular structure of the cation of **2**. Colour code: Mn^{II}, turqoise; Mn^{III}, blue; O, red; N, yellow; C, grey. H atoms and the counter ions are omitted for clarity. [a] Symmetry code: (′) = y, z, x; (″) = z, x, y.

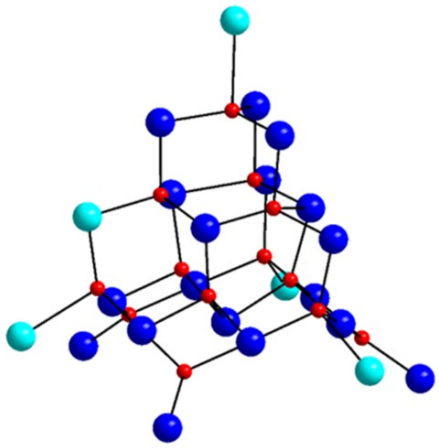

Fig. S5. Representation of the $[Mn^{III}_{18}Mn^{II}_{5}(\mu_4\text{-}O)_{10}(\mu_3\text{-}O)_3]^{38+}$ tricapped supertetrahedral T4 structural core of the cation of **2**. Colour code: Mn^{II}, turqoise; Mn^{III}, blue; O, red. H atoms are omitted for clarity.

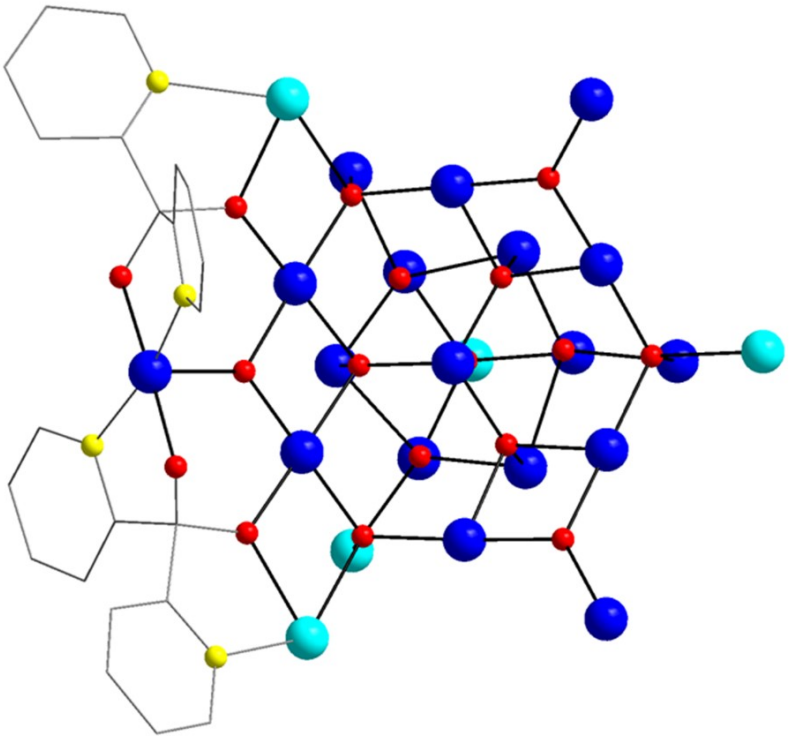

Fig. S6. The connection of the $[Mn_{20}]$ supertetrahedral T4 core of the cation of **2** with a capping Mn^{III} ion through a pair of $\eta^1{:}\eta^2{:}\eta^1{:}\eta^1{:}\mu_3$ $(py)_2C(O)_2^{2-}$ ligands. Colour code: Mn^{II}, turqoise; Mn^{III}, blue; O, red; N, yellow; C, grey. H atoms are omitted for clarity.

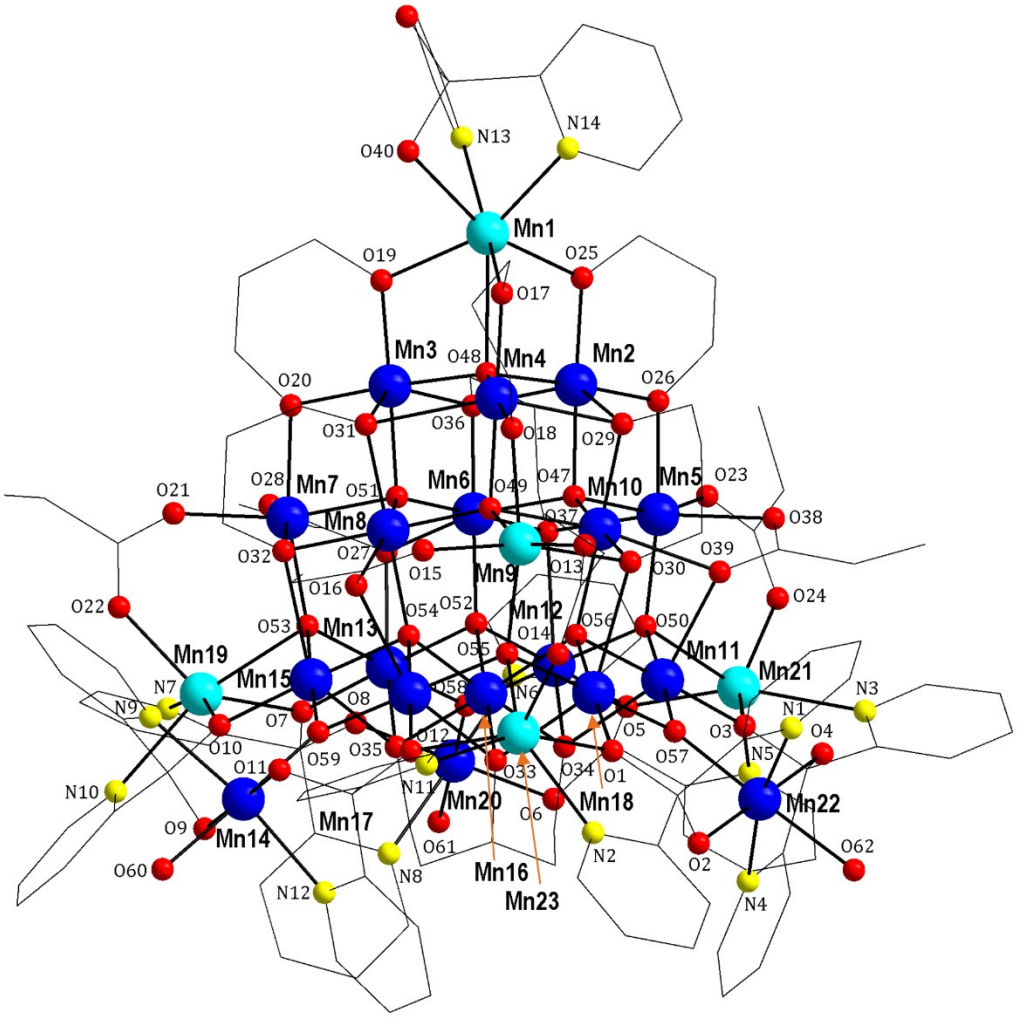

Fig. S7. Partially labeled representation of the molecular structure of the cation of **3**. Colour code: Mn^{II}, turqoise; Mn^{III}, blue; O, red; N, yellow; C, grey. H atoms and the counter ions are omitted for clarity.

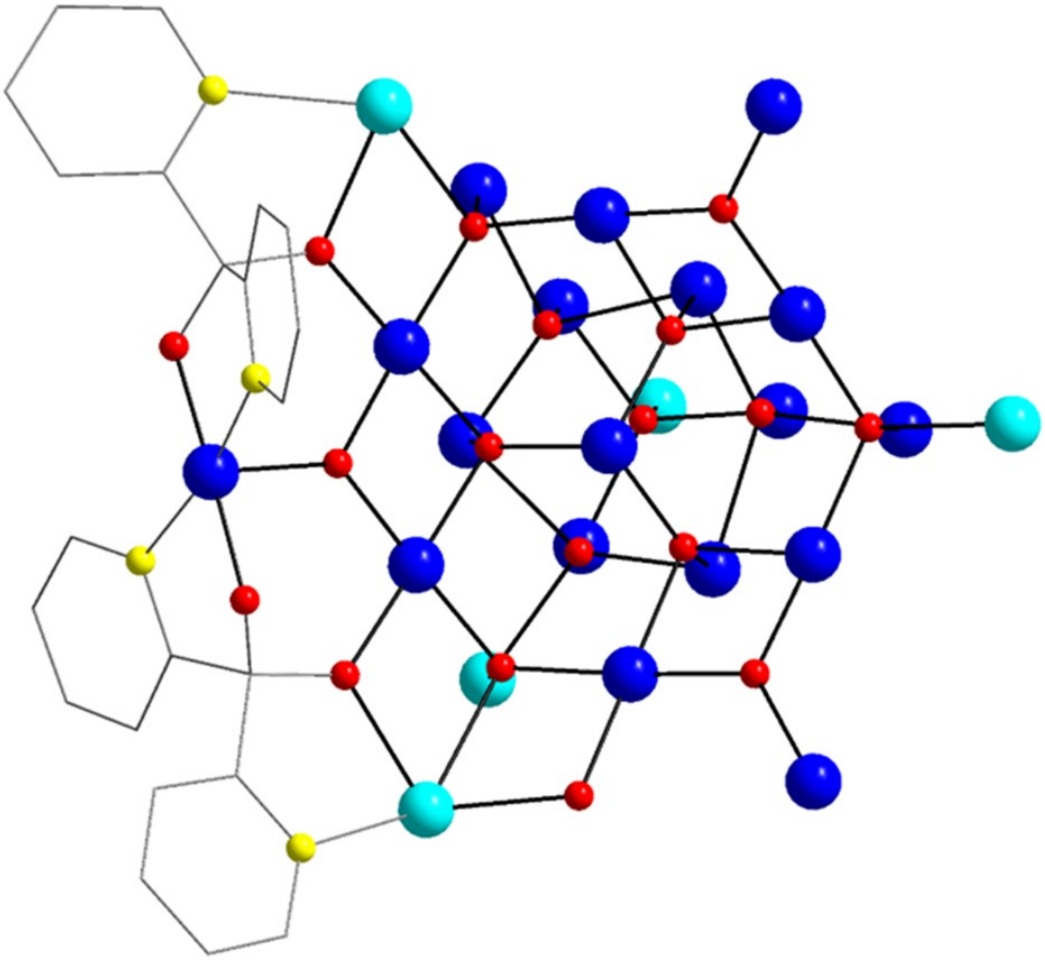

Fig. S8. The connection of the [Mn_{20}] supertetrahedral T4 core of the cation of **3** with a capping Mn^{III} ion through a pair of η^1:η^2:η^1:η^1:μ_3 $(py)_2C(O)_2^{2-}$ ligands. Colour code: Mn^{II}, turqoise; Mn^{III}, blue; O, red; N, yellow; C, grey. H atoms are omitted for clarity.

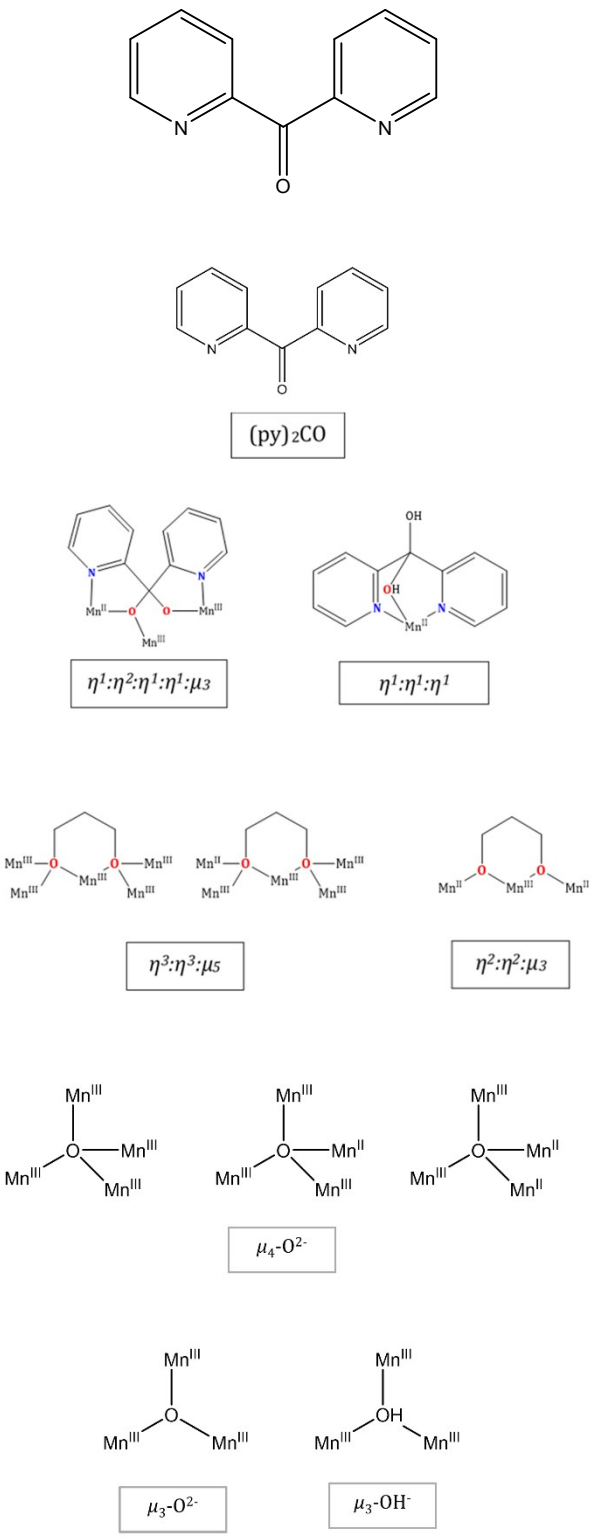

Fig. S9. The ligand $(py)_2CO$ employed in this study and selected examples of coordination modes adopted by $(py)_2C(O)_2^{2-}$, $(py)_2C(OH)_2$, pd^{2-} and O^{2-}/OH^- anions in compounds **1** – **3**.

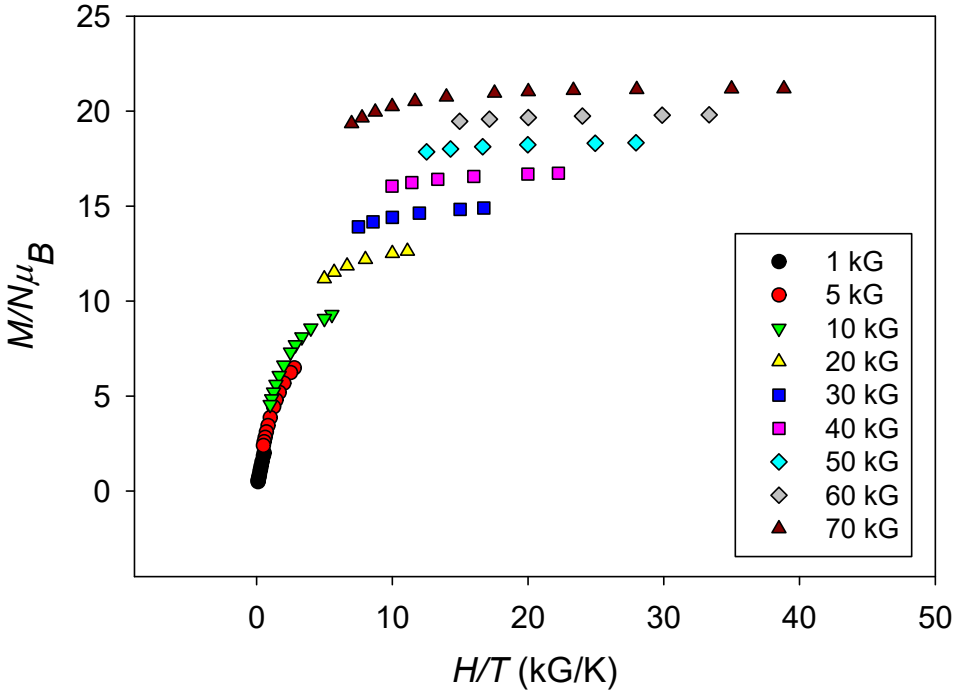

Fig. S10. Plot of reduced magnetization ($M/N\mu_B$) *vs* H/T at the indicated fields for complex **1**·22H_2O.

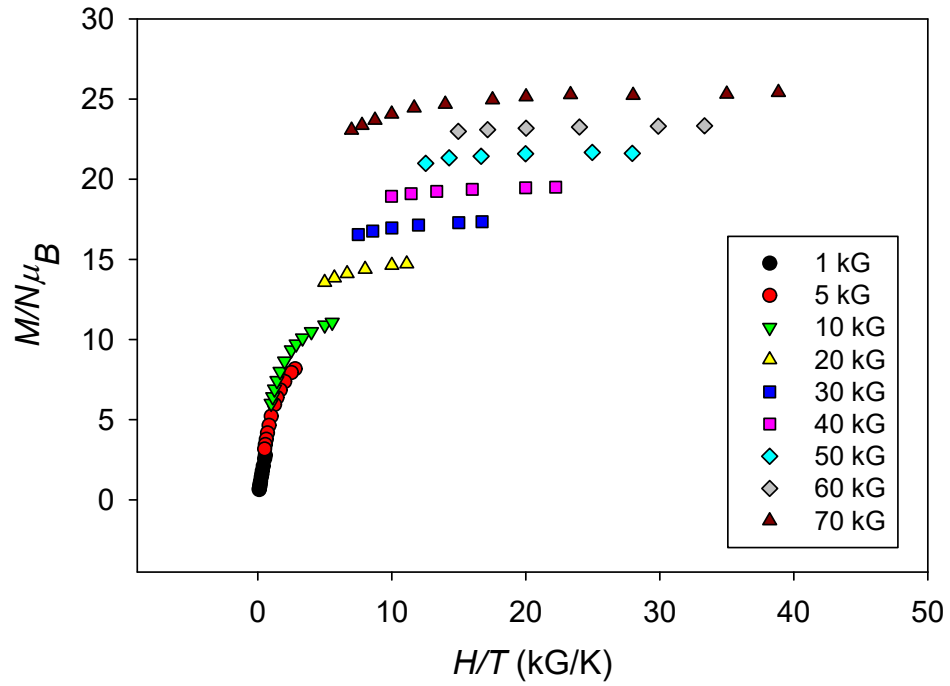

Fig. S11. Plot of reduced magnetization ($M/N\mu_B$) *vs* H/T at the indicated fields for complex **2**·33H_2O.

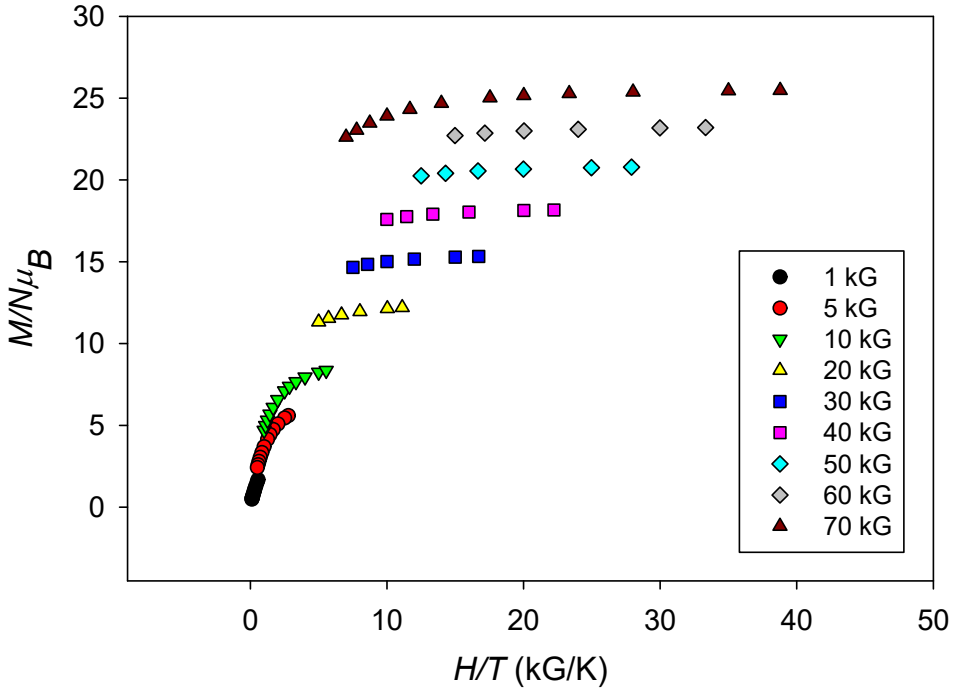

Fig. S12. Plot of reduced magnetization ($M/N\mu_B$) *vs* H/T at the indicated fields for complex **3**·28H_2O.

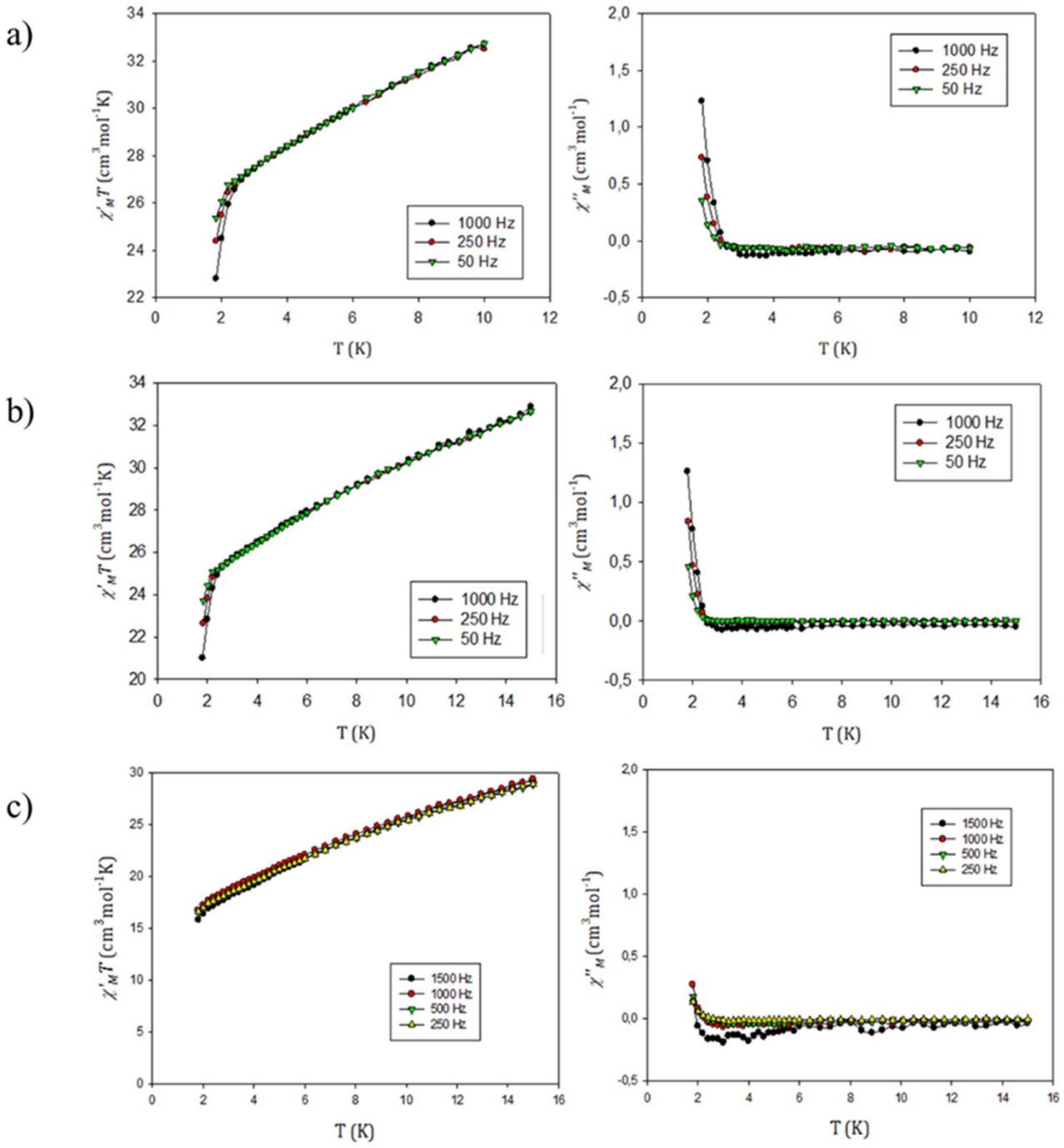

Fig. S13. Plots of the in-phase (χ'_M, as $\chi'_M T$) (left) and out-of-phase (χ''_M) (right) ac magnetic susceptibility versus T for a) **1**·22H_2O, b) **2**·33H_2O and c) **3**·28H_2O at the indicated oscillation frequencies.

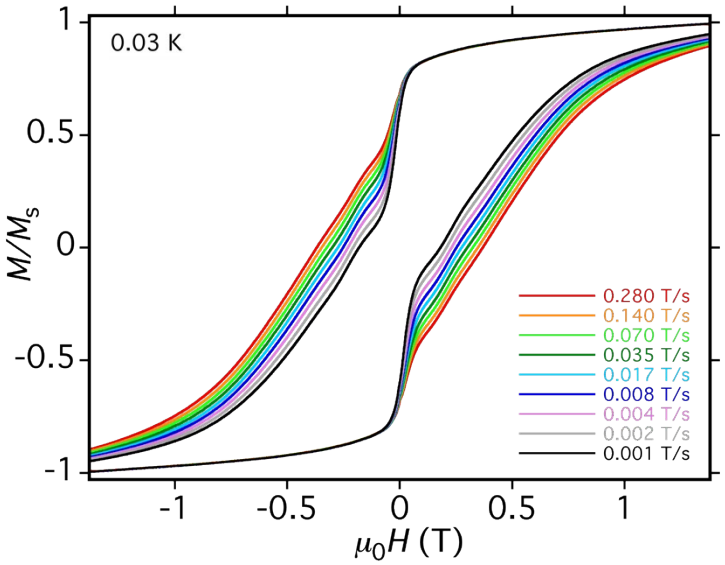

Fig. S14: Magnetization (*M*) versus applied magnetic field ($\mu_0 H$) hysteresis loops for a single crystal of **1**·2.5H_2O·solvent at the indicated field sweep rates and a fixed temperature of 0.03 K. The magnetization is normalized to its saturation value, M_S.

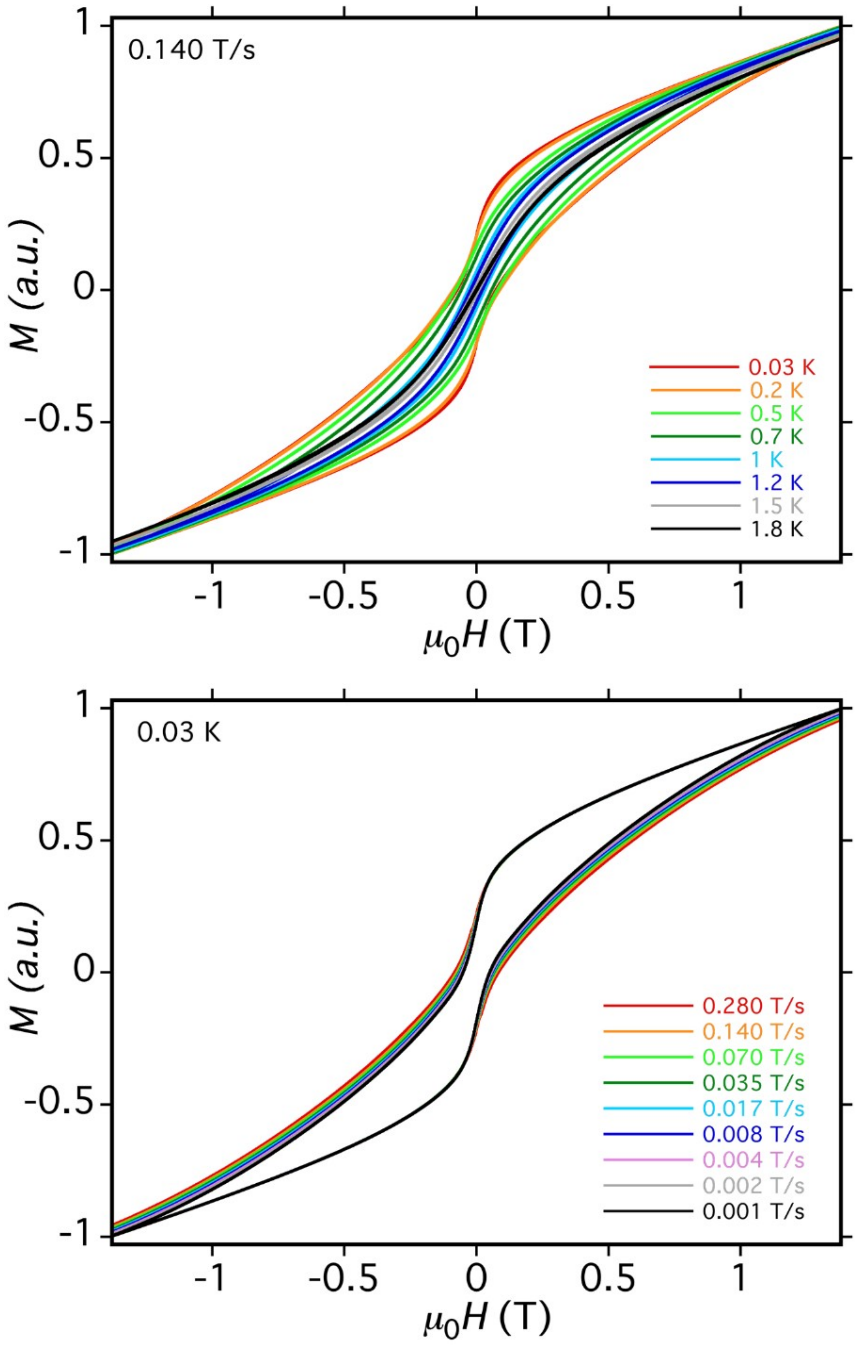

Fig. S15: Magnetization (M) versus applied magnetic field ($\mu_0 H$) hysteresis loops for a single crystal of **2**·3H_2O·solvent at the indicated temperatures and a fixed field sweep rate of 0.140 T s^{-1} (top) and at the indicated field sweep rates and a fixed temperature of 0.03 K (bottom). The magnetization is normalized to its saturation value, M_S.

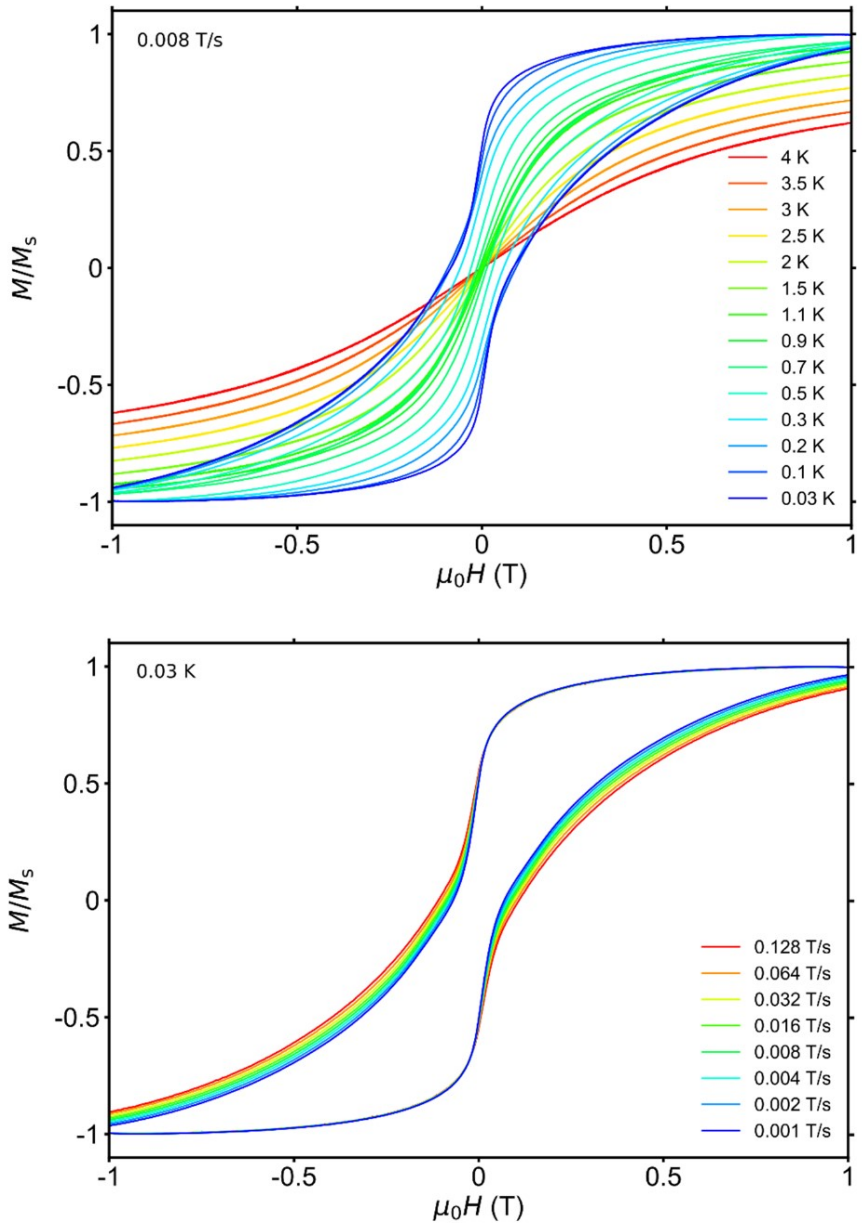

Fig. S16: Magnetization (*M*) versus applied magnetic field ($\mu_0 H$) hysteresis loops for a single crystal of **3**·3.8H_2O·solvent at the indicated temperatures and a fixed field sweep rate of 0.008 T s^{-1} (top) and at the indicated field sweep rates and a fixed temperature of 0.03 K (bottom). The magnetization is normalized to its saturation value, M_S.

References

. T. Lis, *Acta Cryst.*, 1977, **B33**, 2964.
2. J. B. Vincent, H. R. Chang, K. Folting, J. C. Huffman, G. Christou and D. N. Hendrickson, *J. Am. Chem. Soc.* 1987, **109**, 5703.
3. Oxford Diffraction, CrysAlis CCD and CrysAlis RED, version 1.171.32.15, Oxford Diffraction Ltd: Abingdon, England, 2008.
4. M. C. Burla, R. Caliandro, B. Carrozzini, G. L. Cascarano, C. Cuocci, C. Giacovazzo, M. Mallamo, A. Mazzone and G. Polidori, *J. Appl. Cryst.* 2015, **48**, 306.
5. G. M. Sheldrick, *Acta Crystallogr.*, 2008, **A64**, 112.
6. L. J. Farrugia, *J. Appl. Crystallogr.*, 2012, **45**, 849.
7. G.M. Sheldrick, SHELXS version-2018/3 and SHELXL version-2018/3: programs for crystal structure solution and refinement. University of Gottingen, Germany, 2018.
8. O.V. Dolomanov, L.J. Bourhis, R.J. Gildea, J.A.K. Howard, H. Puschmann, *J. Appl. Crystallogr*., 2009, **42**, 339.
9. K. Brandenburg, DIAMOND, Version 3.1d, Crystal Impact GbR: Bonn, Germany, 2006.
10. C. F. Macrae, P. R. Edgington, P. McCabe, E. Pidcock, G. P. Shields, R. Taylor, M. Towler and J. van de Streek, *J. Appl. Crystallogr.*, 2006, **39**, 453.
11. A. L. Spek, *J. Appl. Crystallogr.* 2003, **36**, 7.
12. E. E. Moushi, C. Lampropoulos, W. Wernsdorfer, V. Nastopoulos, G. Christou and A. J. Tasiopoulos, *Inorg. Chem.,* 2007, **46**, 3795.
13. M. Charalambous, E. E. Moushi, C. Papatriantafyllopoulou, W. Wernsdorfer, V. Nastopoulos, G. Christou and A. J. Tasiopoulos, *Chem. Commun*., 2012, **48**, 5410.
14. M. Savva, K. Skordi, A. D. Fournet, A. E. Thuijs, G. Christou, S. P. Perlepes, C. Papatriantafyllopoulou and Anastasios J. Tasiopoulos, *Inorg. Chem.,* 2017, **56**, 5657.
15. E. E. Moushi, T. C. Stamatatos, V. Nastopoulos, G. Christou and A. J. Tasiopoulos, *Polyhedron.,* 2009, **28**, 3203.
16. S. Mukherjee, K. A. Abboud, W. Wernsdorfer and G. Christou, *Inorg. Chem.,* 2013, **52**, 873.